Published in final edited form as:

Mol Microbiol. 2020 September ; 114(3): 495–509. doi:10.1111/mmi.14529.

Interaction with single-stranded DNA-binding protein localizes ribonuclease HI to DNA replication forks and facilitates R-loop removal

Christine Wolak[1], **Hui Jun Ma**[2], **Nicolas Soubry**[2], **Steven J. Sandler**[3], **Rodrigo Reyes-Lamothe**[2], **James L. Keck**[1,‡]

[1]Department of Biomolecular Chemistry, 420 Henry Mall, University of Wisconsin School of Medicine and Public Health, Madison, WI 53706

[2]Department of Biology, McGill University, 3649 Sir William Osler, Montreal, QC, H3G 0B1, Canada

[3]Department of Microbiology, University of Massachusetts, Amherst, MA 01003, USA

Summary

DNA replication complexes (replisomes) routinely encounter proteins and unusual nucleic acid structures that can impede their progress. Barriers can include transcription complexes and R-loops that form when RNA hybridizes with complementary DNA templates behind RNA polymerases. Cells encode several RNA polymerase and R-loop clearance mechanisms to limit replisome exposure to these potential obstructions. One such mechanism is hydrolysis of R-loops by ribonuclease HI (RNase HI). Here, we examine the cellular role of the interaction between *Escherichia coli* RNase HI and the single-stranded DNA-binding protein (SSB) in this process. Interaction with SSB localizes RNase HI foci to DNA replication sites. Mutation of *rnhA* to encode an RNase HI variant that cannot interact with SSB but that maintains enzymatic activity (*rnhAK60E*) eliminates RNase HI foci. The mutation also produces a media-dependent slow-growth phenotype and an activated DNA damage response in cells lacking Rep helicase, which is an enzyme that disrupts stalled transcription complexes. RNA polymerase variants that are thought to increase or decrease R-loop accumulation enhance or suppress, respectively, the growth phenotype of *rnhAK60E rep::kan* strains. These results identify a cellular role for the RNase HI/SSB interaction in helping to clear R-loops that block DNA replication.

Abbreviated summary

DNA replication complexes routinely encounter impediments such as transcription complexes and R-loops that form when RNA hybridizes with complementary DNA templates behind RNA polymerases. We show that interaction between RNase HI and single-stranded DNA-binding protein localizes RNase HI to help clear R-loops that block DNA replication.

[‡]To whom correspondence should be addressed. Telephone: (608) 263-1815, FAX: (608) 262-5253, jlkeck@wisc.edu.

Contributions

CW and SJS performed strain preparation, genetic experiments, growth experiments, SOS assays, and phase contrast microscopy. HJM, NS and RRL performed fluorescence microscopy experiments and the associated strain preparation. CW, RRL, SJS and JLK conceived of experiments. CW, RRL, HJM, NS, SJS, and JLK wrote the manuscript.

Introduction

Replisomes are protein complexes that catalyze high fidelity DNA replication at speeds approaching 1,000 bp/sec in bacteria (Chandler et al.,1975; O'Donnell et al., 2013). During the replication process replisomes encounter numerous impediments to their progress including protein/DNA complexes, non-duplex nucleic acid structures, and chromosomal damage (Mirkin & Mirkin, 2007). To overcome these obstacles, cells have evolved several systems that support replication on imperfect genomic templates. These include enzymes that dissociate protein/DNA complexes and resolve unusual nucleic acid structures, repair pathways that mitigate damaged DNA, and proteins that restructure collapsed replication forks.

RNA polymerase (RNAP) and transcription-dependent nucleic acid structures called R-loops are common barriers to replisome progress (Aguilera & Garcia-Muse, 2012; Helmrich et al., 2013). R-loops are structures that form when a nascent RNA hybridizes with the DNA template behind RNAP (Westover et al., 2004). Bacterial replisomes moves at rates that are ~10-20-times faster than RNAP and can encounter R-loops and/or RNAP from both head-on and co-directional collisions in bacteria (Merrikh et al., 2012). Replication-transcription collisions occur even in eukaryotes, where replication forks move at similar rates to RNAP and most replication and transcription reactions are temporally and spatially separated (Azvolinsky et al., 2009; Helmrich et al., 2011). Head-on collisions can result in replication fork arrest and activation of DNA-damage-dependent recombination (French, 1992; Deshpande & Newlon, 1996; Vilette et al., 1996; Prado & Aguilera, 2005; Mirkin & Mirkin, 2007; Wang et al., 2007). Replisome collisions with RNAP or R-loops can also lead to DNA breaks, genome rearrangements, increased mutagenesis, and activation of DNA damage responses (Huertas & Aguilera, 2003; Li & Manley, 2005; Tuduri et al., 2009; Wahba et al., 2011). These events can create double-strand DNA breaks (DSBs) when a switch in the DNA replication template forms a ssDNA gap that escapes repair prior to the next round of replication (Kuzminov, 2001; Pomerantz & O'Donnell, 2010).

Cells encode redundant pathways to minimize replisome encounters with RNAPs and R-loops and to repair the damage when such collisions occur. These pathways rely on DNA helicases, transcription-associated factors, nucleases, and DNA repair enzymes. One such contributor is ribonuclease HI (RNase HI), an enzyme that hydrolyzes RNA within RNA:DNA hybrids. Classical roles for RNase HI in bacteria include degradation of RNA primers used during DNA replication and suppression of origin-independent chromosomal DNA replication (Itoh & Tomizawa, 1980a; Ogawa & Okazaki, 1980; Ogawa et al., 1984; Alberts, 1987). A more recent role for RNase HI in removing R-loops that block replication forks has been identified (Itoh & Tomizawa, 1980b;Dutta et al., 2011; Merrikh et al., 2012). Genetic relationships link RNase HI with proteins that promote replication fork progression, that repair or restructure replication forks following R-loop induced DNA damage, or that prevent R-loop accumulation (Drolet et al., 1995; Hong et al., 1995; Itaya & Crouch, 1991; Hraiky et al., 2000; Harinarayanan & Gowrishankar, 2003; Sandler, 2005).

Through biochemical and structural studies, a stimulatory interaction formed between *E. coli* RNase HI and the single-stranded DNA binding protein (SSB) has been identified (Petzold

et al., 2015). Stimulation requires docking of the intrinsically-disordered C-terminus of SSB (SSB-Ct) into a binding pocket on RNase HI. This binding mechanism is shared with several other proteins that also form complexes with SSB via the SSB-Ct (Shereda et al., 2008). In some cases, interactions with SSB have been shown to localize its interaction partners to DNA replication forks (Sun & Godson, 1996; Shereda et al., 2008; Marceau et al., 2011).

To probe possible cellular roles of the RNase HI/SSB interaction, we have compared the localization and activity of RNase HI to that of an RNase HI variant that has lost the ability to interact with SSB but that retains normal nuclease activity levels (RNase HI K60E (Petzold et al., 2015)). To do this we created an RNase HI fluorescent fusion protein that forms foci in the cell and colocalizes with a subunit of the DNA replication machinery in *E. coli*. In contrast, the RNase HI K60E fusion variant failed to form foci in *E. coli*. Thus, RNase HI localizes to sites of DNA replication *in vivo* via the interaction with SSB. Strains that substitute the *rnhA* gene (encodes RNase HI) with *rnhAK60E* have normal activities in RNA primer processing and in suppressing origin-independent DNA replication. However, a strain combining *rnhAK60E* with a mutation that inactivates the Rep DNA helicase, an enzyme that helps to promote replisome movement through transcription complexes (Boubakri et al., 2010; Guy et al., 2009), displays a plating deficiency on rich medium and an activated DNA damage response. *rpoB* mutations that produce RNAP variants that are thought to increase or decrease R-loop levels (Kogoma, 1994) enhance or suppress, respectively, the plating deficiency of *rnhAK60E rep::kan* cells. These data lead to a model in which interaction with SSB mediates RNase HI removal of transcription-dependent R-loop obstacles by localizing the enzyme to DNA replication sites.

Results

Interaction with SSB localizes RNase HI to sites of DNA replication in E. coli

SSB is concentrated at replication sites in bacterial cells through its binding to the extended tracts of ssDNA present at DNA replication forks (Meyer & Laine, 1990; Reyes-Lamothe et al., 2010; Reyes-Lamothe, 2012; Marceau, 2012). In some, but not all, instances, direct interaction with SSB also localizes SSB's interaction partner proteins to DNA replication forks (Lecointe et al., 2007; Costes et al., 2010; Bentchikou et al., 2015). To determine whether RNase HI is localized to DNA replication sites in *E. coli*, we created a strain in which the chromosomal *rnhA* locus was replaced with an RNase HI-YPet fluorescent fusion protein and examined RNase HI-YPet focus formation using fluorescence microscopy. RNase HI-YPet foci were found in ~80% of the *E. coli* cells examined, with the majority of cells having either one or two foci (Figure 1A & B). This pattern is strikingly similar to that observed for several fluorescently-tagged DNA replication proteins (Reyes-Lamothe et al., 2008).

To determine whether RNase HI-YPet foci localize to DNA replication forks, the localization of RNase HI-YPet foci and a commonly used replication site marker, mCherry-fused DNA Pol III β-clamp (Reyes-Lamothe et al., 2008; Liu et al., 2010; Reyes-Lamothe et al., 2012; Moolman et al., 2014), were simultaneously measured (Figure 1A). Consistent with RNase HI-YPet foci forming at DNA replication forks, the median distance between a spot of RNase HI-YPet and the nearest mCherry-β-clamp spot is 202 nm (Figure 1C, inset).

These values are slightly higher than those previously reported for replisomal components with the ε subunit of DNA Pol III and β-clamp, which have a median distance of 128 nm (Soubry et al., 2019). Consequently, we further tested for co-localization between RNase HI-YPet and β-clamp-mCherry by comparing the distribution of distances to a random distribution of spots in cells, represented by the radial distribution function *g(r)*. Values of *g(r)* over 1 at short radial distances indicate that the two foci of the proteins overlap far more frequently than randomly distributed spots, supporting co-localization between RNase HI-YPet and β-clamp-mCherry (Figure 1C). In addition, we observed that 16.2% carried spots for β-clamp-mCherry but no RNase HI-YPet, compared with 2.4% of cases for cells with RNase HI-YPet spots but no β-clamp-mCherry, suggesting that RNaseHI is not present at the replication fork at all times or may be present at low levels that are not detected by fluorescence microscopy in some instances.

To better understand the activity of RNase HI, we used single-molecule microscopy to measure the RNase HI copy number per cell and determine the fraction of RNase HI molecules found in foci (Figure S1). To do this, we modified *E. coli* strain AB1157 to encode RNase HI-mNeonGreen at the *rnhA* locus. mNeonGreen was used in place of Ypet as it is currently the brightest monomeric fluorescent protein in use, which maximized detection of single molecules (Shaner et al., 2013). The intensity of a single molecule of RNase HI-mNeonGreen was estimated by measuring the last bleaching step in time traces of foci (Figure S1D & E). Dividing the integrated intensity of a cell by the value of a single molecule, we estimated an average of 82 ± 40 RNase HI molecules per *E. coli* cell (Figure S1F), of which 20 ± 13% were localized in foci (Figure S1). These data suggest that in many instances there are multiple copies of RNase HI localized in foci. In addition, a significant number of RNase HI molecules are available in the diffusive pool.

Prior structural and biochemical experiments defined the SSB-binding site on RNase HI and identified a point mutation in RNase HI (K60E) that eliminated interaction without altering nuclease activity *in vitro* (Petzold et al., 2015). The cellular localization of RNase HI K60E-YPet was examined next to determine whether RNase HI-YPet focus formation requires interaction with SSB. Unlike RNaseHI-YPet, foci were not observed for RNase HI K60E-YPet and the fluorescence signal of the variant was distributed throughout the cell (Figure 1D). This result indicates that RNase HI/SSB complex formation is necessary for recruitment and/or retention of RNase HI at DNA replication sites in *E. coli*.

SSB-mediated localization of RNase HI is not required to suppress origin-independent replication or to degrade lagging-strand Okazaki fragment primers

RNase HI has noted activities in three major cellular processes in *E. coli*: (*1*) suppression of origin-independent “constitutive stable DNA replication” (cSDR), (*2*) degradation of lagging-strand RNA primers used during DNA replication, and (*3*) removal of R-loop replication barriers. To test for possible roles of SSB-mediated localization of RNase HI in each of these activities, we created an *E. coli* strain with a mutated *rnhA* locus that encodes for the RNase HI K60E variant (*rnhAK60E*) and compared its phenotype to otherwise isogenic *rnhA*+ and *rnhA::cat E. coli* strains (Table S1). *E. coli* with the *rnhAK60E* mutation were phenotypically indistinguishable from *rnhA*+ and *rnhA::cat* cells in terms of growth

rate, cell morphology and rich medium plating efficiency (Figures 2, 3 & S2). Given the lack of a phenotypic difference for the *rnhA* point mutation, we next combined the *rnhAK60E* mutation with mutations in other genes that have established genetic relationships with *rnhA* to test whether loss of RNase HI/SSB complex formation affects the pathways in which RNase HI is involved.

We first examined whether the *rnhAK60E* mutation impacted RNase HI suppression of cSDR in *E. coli*. In cSDR, R-loops are processed by RecA, DNA polymerase I and the primosome to allow for replication initiation away from *oriC*. RNase HI nuclease activity regulates this process by removing R-loops before the replisome can be loaded (Tokio Kogoma, 1978; von Meyenburg et al., 1987). Therefore the inactivation of *rnhA* preserves R-loops and can rescue cell growth in strains carrying otherwise lethal mutations in the *oriC*-replication initiation pathway (*e.g. dnaA* loss of function mutants) (Frey et al., 1981; Kogoma & von Meyenburg, 1983; de Massy et al., 1984; Lindahl & Lindahl, 1984; von Meyenburg et al., 1987; Carr & Kaguni, 1996). To test whether abrogation of SSB-mediated RNase HI localization facilitates cSDR similarly to *rnhA::cat*, we introduced the *rnhAK60E* allele into *dnaA46(ts)* cells. Similarly to *rnhA+ dnaA46(ts)*, the *rnhAK60E dnaA46(ts)* strain was unable to grow under non-permissive conditions (42 °C), whereas the *rnhA::cat dnaA46(ts)* strain was able to grow at 42 °C (Figure S3). This result indicates that the RNase HI K60E variant maintains sufficient activity to remove R-loops required for cSDR. Thus, SSB-mediated localization of RNase HI is not required for inhibiting R-loop dependent replication initiation.

We next tested whether SSB-mediated RNase HI localization was important for degrading RNA primers used during canonical DNA replication. The nuclease activities of RNase HI and DNA polymerase I work together to remove RNA primers that initiate lagging-strand Okazaki fragments (Ogawa & Okazaki, 1984; Kitani et al., 1985; Crouch, 1990). Inactivation of *rnhA* leads to media- and temperature-dependent impaired growth of an *E. coli* strain carrying the *polA12(ts)* allele, which encodes a DNA polymerase I variant that has strongly reduced 5'-3' exonuclease and polymerase activities at 42 °C (Uyemura & Lehman, 1976; Joyce et al., 1985;). To determine whether binding to SSB is required for primer-degradation by RNase HI, growth of a strain combining the *rnhAK60E* mutation with *polA12*(ts) was compared to *rnhA+ polA12*(ts) and *rnhA::cat polA12*(ts) strains. Growth of *rnhAK60E polA12(ts)* cells was indistinguishable from *rnhA+ polA12*(ts) cells at 30 or 42 °C in rich or minimal media (Figure S4). In contrast, the *rnhA::cat polA12*(ts) strain displayed media- and temperature-dependent growth defects as previously reported (Uyemura & Lehman, 1976; Joyce et al., 1985;). These data indicate that SSB-mediated RNase HI localization is not required for Okazaki fragment RNA primer processing.

Genetic interactions of rnhAK60E with DNA helicases

To examine the role of the RNase HI/SSB interaction in additional replication and repair processes, we tested the effects of combining *rnhAK60E* with deletions in several DNA replication/repair genes: *rep*, *recBCD*, *recG, uvrD*, or *dinG* (Table 1). These were chosen based on the reported synthetic lethal effects of *rnhA* deletion with *rep* (Sandler, 2005), *recBCD* (Itaya & Crouch, 1991; Kogoma et al., 1993; Hong et al., 1995; Kogoma, 1997b;),

and *recG* (Hong et al., 1995) deletions and the proposed roles of UvrD and DinG helicases in DNA replication fork maintenance or repair (Kornberg & Baker, 1992; Sandler et al., 1996; Michel, 2005; Srivatsan et al., 2010; Boubakri et al., 2010; Dimude et al., 2015). Inactivation of several of these genes along with *rnhA* increases the possibility of collisions between replisomes and transcription-dependent R-loops and/or diminishes the capacity of cells to repair the resulting DNA damage from replication fork collapse (Kogoma et al., 1994; Hraiky et al., 2000; Wahba et al., 2011; Merrikh et al., 2012; Dimude et al., 2015).

We first measured the co-transduction frequencies of *rep::kan*, *recBCD::cat*, or *recG::kan* into three strains with different *rnhA* backgrounds: *rnhA+*, *rnhAK60E,* or *rnhA::cat*. *rep::kan*, *recBCD::kan,* and *recG::cat* each transduced with similar frequencies into *rnhA+* and *rnhAK60E* strains whereas they failed to transduce into *rnhA::cat* cells (Table 1). Another observation to note was that the *rnhA::cat rep::kan* synthetic lethality was dependent on transduction direction, a trait not observed with other synthetic lethal pairs (Table 1). This could be due to background differences between the *rep::kan* strain and the *rnhA* strains used in our study.

We expanded our screen to examine deletions of two other helicase genes: *uvrD::kan* and *dinG::kan.* The *uvrD::kan rnhA::cat* combination was synthetically lethal whereas the *dinG::kan rnhA::cat*, *uvrD::kan rnhAK60E*, and *dinG::kan rnhAK60E* strains were viable and had similar co-transduction frequencies to those observed with the *rnhA+* recipient (Table 1). Synthetic lethality of the *uvrD::kan rnhA::cat* is interesting considering recent data demonstrating that UvrD has a direct role in promoting replication fork movement past transcription collisions whereas DinG operates more indirectly and could reduce the chance of collisions (Hawkins et al., 2019).

These results indicate that the *rnhAK60E* mutation is not synthetically lethal with *rep*, *recBCD*, *recG*, uvrD, or *dinG* deletions (Table 1). Thus, loss of RNase HI localization conferred by the *rnhAK60E* mutation is not synonymous with a loss of RNase HI activity when combined with mutations in DNA replication and repair helicases. Nonetheless, the viability of the *rnhAK60E* variant in these helicase mutant strains allowed us to probe the role of the RNase HI/SSB interaction under other cellular conditions.

The rnhAK60E rep::kan strain is sensitive to rich medium and is induced for SOS

Although the co-transduction experiments did not reveal synthetic lethal combinations between *rnhAK60E* and several different DNA repair gene deletions, a media-dependent growth defect was detected specifically with the *rnhAK60E rep::kan* strain (Figure 2). The *rnhAK60E rep::kan* strain plated with the same efficiency as wild-type, rnhAK60E, or *rep::kan* strains on minimal medium (normalized to OD_{600} (CFU/mL/OD)) but the double mutant has an approximately 10-fold reduced plating efficiency on LB after 24 hours relative to the other strains (Figure 2). The lower plating efficiency on LB improves somewhat after 48 hours, indicating that the phenotype is due to slow growth rather than cell death (Figure 2). Interestingly, the slow growth defect of *rnhAK60E rep::kan* cells is not obvious in liquid growth curves (Figure S2). Slow growth was unique to the *rnhAK60E rep::kan* strain since the other strains that were synthetic lethal with *rnhA*::cat (*uvrD::kan, recG::kan,*

recBCD::cat) plated with indistinguishable efficiencies on minimal and LB plates with the *rnhAK60E* mutation (Figure S5).

With the increased frequency of DNA replication and other stresses that arise in rich nutrient conditions, rich-medium dependent growth defects can be indicative of dysfunctional genome maintenance pathways (Boubakri et al., 2010; Srivatsan et al., 2010). Such problems can also lead to an increase in DNA damage that induces the SOS response, a survival mechanism used by *E. coli* to regulate the expression of DNA repair genes (Janion, 2008; Walker et al., 2000; Michel, 2005). To test whether loss of RNase HI replication fork localization and/or Rep helicase activity induces the SOS response in *E. coli*, the strains were transformed with a reporter plasmid that has a *recN* promoter-GFP fusion (Chen et al., 2015) and GFP levels were measured during exponential growth. *recN* is among the first group of genes to be induced during SOS, making its expression an indicator of SOS status (Finch et al., 1985; Rostas et al., 1987).

The SOS level of the *rnhAK60E* strain was indistinguishable from wild-type cells in minimal and rich media whereas the *rep::kan* strain had ~3.5-fold higher GFP levels in both minimal and rich media (Figure 3). Interestingly, combining the *rnhAK60E* and *rep::kan* mutations resulted in the same GFP levels as the *rep::kan* strain in minimal medium but the GFP levels were 3.3-fold higher than *rep::kan* in rich medium. The rich medium-specific increase in SOS response for *rnhAK60E rep::kan* cells correlates with reduced plating efficiency for the strain on LB.

Cell morphologies of the strains were examined to determine whether they demonstrated signs of cell filamentation, a phenotypic consequence for the SOS response. *rnhAK60E* and *rep::kan* cells had lengths that were similar to wild-type *E. coli*, however, the *rnhAK60E rep::kan* cells were more frequently filamented (Figure 3B & C). In minimal medium, *rnhAK60E rep::kan* cells were slightly elongated in comparison to wild-type cells whereas growth in rich medium led to much more extreme cell filamentation (p-value < 0.001) (Figure 3B & C). These data show that abrogation of SSB-mediated RNase HI localization to the replication fork along with a loss of Rep helicase activity leads to an increase in DNA damage stress.

The rnhAK60E rep::kan phenotype is related to transcription-dependent R-loop removal.

RNase HI can remove transcription-dependent R-loops and the Rep helicase helps the replication fork progress through protein obstacles including stalled transcription complexes (Kogoma, 1978; Itoh & Tomizawa, 1980b; von Meyenburg et al., 1987; Guy et al., 2009; Boubakri et al., 2010). With the result that RNase HI is localized to the replication fork through interaction with SSB, it is possible that RNase HI and Rep collaborate to promote replisome progression when faced with R-loops and transcription complexes (Drolet et al., 1995; Hraiky et al., 2000; Boubakri et al., 2010; Dutta et al., 2011; McGlynn et al., 2012). To further test this hypothesis, we examined whether changes in RNAP activity impact the growth phenotype of *rnhAK60E rep::kan* cells. Two RNAP β subunit mutations were chosen for the analysis: *rpoB2* is defective in termination whereas *rpoB8* has a slower elongation rate than wild-type and is prone to termination (Jin et al., 1988; Jin et al., 1992). A previous study showed that combining an *rnhA* deletion with *rpoB2* leads to a plating defect on rich

medium and elevated SOS whereas combining an *rnhA* deletion with *rpoB8* reduces SOS levels (Kogoma, 1994). These effects are thought to arise from *rpoB2* and *rpoB8* mutant RNAPs generating more or fewer R-loops, respectively, than wild-type RNAP, and with the abundant R-loops in the *rpoB2 rnhA*- cells acting as barriers that slow replication (Kogoma, 1994).

Consistent with the model for synergy between RNAP and RNase HI/Rep, a *rnhAK60E rep::kan rpoB2* strain had a worsened plating efficiency relative to *rnhAK60E rep::kan* cells on both LB and minimal media plates (Figure 4). Even after a 48 hour incubation period the *rnhAK60E rep::kan rpoB2* CFUs on LB did not increase (Figure 4). In contrast, the *rnhAK60E rep::kan rpoB8* strain had the same plating efficiency as wild-type cells on minimal medium and LB, indicating that the *rpoB8* mutation suppressed LB growth sensitivity in *rnhAK60E rep::kan* cells. When either *rnhAK60E* or *rep::kan* were combined individually with the *rpoB* point mutations there were no significant changes in the plating efficiency relative to *rpoB2* or *rpoB8* cells (Figure S6). These data demonstrate that an RNAP variant that is thought to produce high levels of R-loops exacerbates the impact of losing RNase HI localization and Rep helicase activity whereas an RNAP variant that reduces cellular R-loop levels counteracts the mutations.

Discussion

E. coli RNase HI forms a direct interaction with SSB that stimulates RNase HI enzymatic activity *in vitro* (Petzold et al., 2015). In this report, the cellular roles of the RNase HI/SSB interaction have been examined. An *E. coli* RNase HI fluorescent fusion protein forms foci in cells whereas an enzymatically-active variant that cannot interact with SSB (RNase HI K60E) does not form foci. RNase HI foci colocalize with a component of the replisome, consistent with SSB-dependent accumulation of the enzyme at DNA replication sites in *E. coli*. The RNase HI K60E variant supported RNase HI-mediated suppression of cSDR and lagging-strand RNA primer degradation, indicating that localization was not required for these cellular functions. In contrast, cells encoding RNase HI K60E displayed a media-dependent plating defect and an activated SOS response when the gene encoding the Rep DNA helicase was deleted. This phenotype was linked to a deficiency in resolving transcription-derived R-loops by examining the effects of RNAP mutations that alter R-loop levels (Jin et al., 1988; Jin et al., 1992) on *rnhAK60E rep::kan* cells. Adding *rpoB2*, which is thought to increase the abundance of R-loops (Kogoma, 1994), further increased the plating defect of *rnhAK60E rep::kan* cells whereas adding *rpoB8*, which is thought to decrease R-loop abundance, suppressed the growth phenotype. These results support a model in which SSB-dependent replication fork localization of RNase HI assists in replication progression through transcription-derived R-loops.

Roles for RNase HI in resolving replication/transcription conflicts have been proposed, but the precise mechanisms that allow RNase HI to target specific R-loop challenges to replication fork progression have not been defined (Drolet et al., 1995; Hraiky et al., 2000; Li & Manley, 2005; Tuduri et al., 2009; El Hage et al., 2010; Gan et al., 2011; Dutta et al., 2011; Houlard et al., 2011; Wahba et al., 2011). Our results support a model in which binding to SSB recruits RNase HI to sites of replication in *E. coli*, which positions the

enzyme to degrade R-loop impediment. Several other cellular factors that resolve R-loop/RNAP blockages similarly rely on protein interactions for recruitment to their site of action to mediate replication progress. These include Rep, DinG, and UvrD helicases in *E. coli,* that directly associate with RNAP or with replication fork-bound proteins (Trautinger et al., 2005; Baharoglu et al., 2010; Boubakri et al., 2010; Proshkin et al., 2010; Tehranchi et al., 2010; Dutta et al., 2011; Washburn & Gottesman, 2011). Rep is localized to sites of replication by interaction with the replicative DnaB helicase and DinG binds to SSB (Guy et al., 2009; Boubakri et al., 2010; Atkinson et al., 2011; Cheng et al., 2012; Syeda et al., 2019). UvrD associates with RNAP, which may aid in its removal of stalled transcription complexes or resolution of replication/transcription conflicts through other mechanisms (Epshtein et al., 2014; Hawkins et al., 2019; Kamarthapu et al., 2016; Sanders et al., 2017).

Our results show that simultaneous mislocalization of RNase HI and loss of Rep helicase result in defects in *E. coli* growth that are dependent on R-loop production by RNAP. Interestingly, full deletion of *rnhA* and *uvrD* is synthetically lethal as well (Table 1), but, unlike the situation with Rep, RNase HI mislocalization in the *rnhAK60E* mutant did not result in a measurable phenotype when coupled with a *uvrD* deletion (Table 1 and Figure 2). Furthermore, *dinG* was able to be deleted from an *rnhA*-deleted strain, consistent with a recent study suggesting that DinG may act less directly to resolve replication/transcription conflicts (Hawkins et al., 2019). Our results suggest that RNase HI functions synergistically with Rep, and likely UvrD to a lesser extent, to promote genome duplication through R-loop-dependent fork obstacles.

How might SSB-medicated RNase HI localization help to remove R-loop obstacles to the replication fork? In *E. coli*, the lagging strand template is exposed as ~1-2 kb long ssDNA segments at replication forks. SSB binding to this ssDNA positions numerous SSB molecules at each site of DNA replication (Figure 5). Since each SSB tetramer has four SSB-Ct protein interaction sites, the SSB/ssDNA structures at replication forks offers abundant bindings sites for partner proteins at each fork. As has been shown here, RNase HI forms foci at replication sites in a manner that requires interaction with SSB (Figure 1); several other SSB protein partners localize to the replication fork in the same manner (Sun & Godson, 1996; Glover & McHenry, 1998; Marceau et al., 2011; Wessel et al., 2013; Bhattacharyya et al., 2014). Thus, the interaction poises RNase HI at replication forks to concentrate its nuclease activity to loci adjacent to the advancing fork. Our data collectively support a model in which this localization allows RNase HI to hydrolyze R-loops encountered ahead of the replication fork to aid in clearing RNAP complexes that would otherwise impede replication progression. With its noted roles in clearing RNAP (Guy et al., 2009; Boubakri et al., 2010), Rep helicase appears to cooperate with RNase HI in this activity.

We note that SSB might also coat the exposed DNA strands of R-loops and that such an arrangement could also assist with recruiting RNase HI to R-loops. Since this would also impact cSDR and no deficiency in RNase HI inhibition of cSDR was detected with the RNase HI K60E variant, this recruitment strategy does not appear to be as important as the localization to replication forks for resolving replication/transcription conflicts.

The observations described here highlight parallels between bacterial RNase HI and human RNase H1 noted in recent studies. Human RNase H1 directly interacts with Replication Protein A, the functional equivalent of bacterial SSB, forming a complex that stimulates the activity of RNase H1 *in vitro* and that is critical for suppression of R-loop forming *in vivo* (Nguyen et al., 2017). Additionally, depletion of human RNase H1 leads to an accumulation of R-loops, slowed replication fork progression, and increased DNA damage (Parajuli et al., 2017). It therefore appears that SSB-mediated RNase H localization is a general phenomenon that cells have adapted to facilitate progression through R-loop challenges to replication processes in both bacterial and eukaryotic cells.

Experimental Procedures

Bacterial strains and growth

All bacterial strains are derivatives of *E. coli* K12 and are described in Table S1. Mutations were introduced into the strain of interest by P1 transduction (Willetts et al., 1969). P1 transductions were selected on 2% agar plates made with Luria broth (LB) or 56/2 minimal medium (Willetts et al., 1969). M9 was supplemented with glycerol (final concentration 0.2%); 100 μg/ml of amino acids threonine, leucine, proline, histidine and arginine; and thiamine (0.5 μg/ml). Ampicillin (10 μg/mL), tetracycline (10 μg/mL), kanamycin (50 μg/mL), chloramphenicol (25 μg/mL; 12.5 μg/mL for electroporation selection), rifampicin (50 μg/mL) were added when required. Mutations were confirmed after new strain generations by colony PCR and sequencing.

Strain preparation

General procedure for constructing the *rnhAK60E* chromosomal point mutation followed the λ-Red recombination method (Datsenko & Wanner, 2000). The *rnhA* gene was placed onto a pET15b with a 10 nt gap and Cm^r cassette on the 3′ to generate the following product: pET15b-rnhA-10nt – FRT-cat- FRT. The pET15b-*rnhA* plasmid was used as a template for site directed mutagenesis as previously described to make the K60E point mutation (Petzold et al., 2015). In addition to the point mutation a restriction site polymorphism (XhoI) was inserted adjacent to K60E to allow for screening of the allele. Electrocompetent BW25113 cells with pKD46 (Datsenko & Wanner, 2000) were used to electroporate the *rnhA-cat* and *rnhAK60E-cat* DNA fragments. Cells that had incorporated the DNA were selected on LB with 12.5ug/mL chloramphenicol (LB + Cm). Colonies were purified on LB + Cm and colony PCR was performed on Cm^r transformants to confirm the incorporation of Cm^r cassette. For cells transformed with *rnhAK60E-cat* a restriction digest with XhoI was also used to check for the point mutation. Cells with the correct product size were sequenced at the *rnhA* locus by colony PCR. P1 lysates were prepared from *rnhA-cat* and *rnhAK60E-cat* cells and introduced into JC13509 selecting for Cm^r. The protocol for P1 transduction has been described previously (Willetts et al., 1969). The Cm^r transductants were again sequenced to confirm the *rnhA* genotype. The protocol for removing Cm^r was performed as described in (Datsenko & Wanner, 2000).

All strains used for microscopy are AB1157 derivatives. Strain carrying a wildtype copy of RNase HI fused to YPet (RRL327) or mNeonGreen (VV14) were generated through lambda

red recombination as previously described (Reyes-Lamothe et al., 2008). Briefly, primers L_rnhA_F (ccgcggcgatgaatcccacactggaagatacaggctaccaagttgaagttTCGGCTG GCTCCGCTGCTGG) and L_rnhA_R (cgaattcgccaggcggttggagccacccggcaatgtcgtaaacc acaggcCTTATGAATATCCTCCTTAG) and were used to amplify *ypet* and kan^R from the plasmid pROD61 or *mneongreen* and kan^R from the plasmid plasmid pVV04. Integration into the chromosome was done using plasmid pKD46, which expresses the lambda red genes under the control of arabinose (Datsenko & Wanner, 2000). The strain carrying the *rnhAK60E* allele fused to *ypet* (VV8) was generated by cloning *rnhA-ypet kan* with ~500 bp of flanking regions at either side, amplified from RRL327, into a plasmid carrying an R6K gamma origin using primers rnhA_seqF5 (TTTAGACGTCGGCTATCGGTGACCTTACAG) and rnhA_seqR3 (ATCAAGTGAATGTTTCTGCGC) (resulting in pVV10). Cloning was done using an AatII site at one end and TA cloning at the other end, and ligated into a fragment containing the R6K gamma origin amplified from pKD4 (Datsenko & Wanner, 2000). The point mutation was introduced by Quick Change mutagenesis using primers rnhA_K3EF (GCGCTGGAGGCGTTAGAAGAACATTGCGAAGTC) and rnhA_K3ER (GACTTCGCAATGTTCTTCTAACGCCTCCAGCGC). The resulting *rnhAK60E-ypet kan* was introduced in the chromosome, replacing the wildtype copy, using primers rnhA_seqF3 (GGCTATCGGTGACCTTACAG) and rnhA_seqF3.

The *mcherry-dnaN* fusion (RRL355) was constructed by lambda red using primers dnaN-NF (TATCAAAGAAGATTTTTCAAATTTAATCAGAACATTGTCATCGTAAACCTGTAGGC TGGAGCTGCTTCG) and dnaN-NR (ACCTGTTGTAGCGGTTTTAATAAATGCTCACGTTCTAC GGTAAATTTCATCGCGCTGCCAGAACCAGC) and pROD84 as a template, carrying a kan^R *mcherry* followed by an 11 amino acid linker. The kanamycin cassette was removed by FLP recombinase expression from pCP20 (Datsenko & Wanner, 2000) resulting in strain RRL388. Fluorescent *rnhA-ypet* kan^R fusion was moved into the strain carrying RRL388 by P1 transduction (resulting in strain VV11).

Growth curves

Strains were inoculated from single colonies in overnight liquid cultures of 56/2 minimal media with antibiotic where relevant (Willetts et al., 1969). After growth at 37°C for 16h, overnight cultures were used to inoculate 25mL of LB or 56/2 minimal media (100-fold dilution). OD_{600} was taken at t=0 and at subsequent 30 minute time points until several time points at stationary phase was reached. Time points from three independent experiments were plotted with standard deviation using GraphPad Prism.

CFU/mL/OD_{600} determination

Strains were inoculated from single colonies in overnight liquid cultures of 56/2 minimal medium with antibiotics when relevant (Willetts et al., 1969). After growth at 37°C for 16h the OD_{600} of overnight cultures was taken. Cultures were serially diluted in sterile saline and 10μL of the appropriate dilution was plated on LB or 56/2 minimal media. Colony counts were performed after the plates were incubated at 37°C for 24h and 48h. CFU/ml/OD_{600} values were determined by the following equation: [(dilution factor/volume plated) * colony

count]/ OD_{600}. CFU/ml/OD_{600} values were accumulated for at least three independent cultures and plotted with standard deviation using GraphPad Prism.

Phase Contrast Microscopy

Strains were inoculated from single colonies in overnight liquid cultures of 56/2 minimal medium with 100μg/mL ampicillin (Willetts et al., 1969). After growth at 37°C for 16h the overnight cultures were diluted 100-fold in 56/2 minimal medium or LB with ampicillin. 4μL of cells were spotted on fresh 2% agarose pads (1XPBS) and covered with a coverslip. Cells were imaged at 25°C using an inverted Nikon Eclipse Ti microscope equipped with a Photometrics CoolSNAP HQ2 charge-coupled-device (CCD) camera (Photometrics, Tucson, AZ). Images were acquired using a ×100 oil objective (Nikon Plan Apo 100/1.40 oil Ph3 DM) and the Nikon Instruments Software (NIS)-Elements Advanced Research (AR) microscope imaging software program (Version 4.000.07) (Nikon, Melville, NY). Data were collected on the EMCCD using an exposure time of 50 ms. Data from at least 200 cells from three independent cultures was collected and analyzed using MicrobeTracker to determine average cell length for each strain in minimal and rich media (Sliusarenko et al., 2011).

Fluorescence Microscopy

Imaging was performed at room temperature on an inverted Olympus IX83 microscope using a 100x oil objective lens (Olympus Plan Apo 100X NA 1.40 oil). Images were captured using an Andor Zyla 4.2 sCMOS camera. Z-stacks were done using a NanoScanZ piezo by Prior Scientific. Excitation was done from an iChrome Multi-Laser Engine (405nm 100mW, 488nm 100mW, 561nm 100mW, 640nm 70mW) from Toptica Photonics and a 405/488/561/640nm filter set (Chroma). Laser triggering was done through a real-time controller U-RTCE (Olympus). Experiments were done from a single-line cellTIRF illuminator (Olympus). Olympus CellSens 2.1 imaging software was used to control the microscope and lasers.

Before imaging cells were grown in LB for at least 5 hours then transferred to M9-Glycerol medium via a 1:1000 dilution. After being grown overnight cells were diluted again in M9-Glycerol and grown to an OD_{600} between 0.1- 0.2. Cells were spotted on a 1% agarose pad in M9-Glycerol. Imaging of YPet strains was done capturing for 500ms with 15% laser power (488nm laser), while imaging of mCherry was done using 500ms with 13% laser power (561nm laser). At each field of view a z-stack of 32 pictures with a 100nm step size was taken using brightfield illumination, which was later used for segmentation.

Spot counting and colocalization analysis

All analysis was done using custom scripts written in MATLAB (Mathworks). A 32-frame bright field Z-stacks was compressed to create a black and white phase contrast image for cell segmentation (Julou et al., 2013). Cells were segmented using SuperSegger software (Stylianidou et al., 2016). Spots were counted using a modified version of the previously developed tracking software (Uphoff et al., 2013). Spots were determined using an intensity threshold then further processed using a 2D-elliptical Gaussian fit. The extracted fitted parameters were; x-position, y-position, x-standard deviation, y-standard deviation, intensity and background. Co-localization analysis was done by measuring the distance between the

positions of ribonuclease HI-YPet to the β-clamp-mCherry in two-colour experiments. If cells had multiple foci of the same protein, then the smallest distance was recorded, and the 2 spots measured removed so their positions would not be used again in further calculations.

Colocalization was characterized using radial distribution analysis (Zawadzki et al., 2015; Thrall et al., 2017). The radial distribution function *g(r)* displays the increased likelihood of ribonuclease HI-YPet at a distance *r* from a mCherry-β-clamp focus relative to random cellular localization. This measurement incorporates the cell shape and size of the cells analysed in the colocalization analysis. An equivalent number of random localizations were generated within the cell outline and the distance between them and the position of a β-clamp-mCherry focus (obtained from the data for a particular cell in the analysis) measured. We also measured the distance between two randomly generated localizations in the cell. This procedure was repeated for each cell. To account for variability, we simulated the single protein random localization and two protein random localization distributions 100 times. We then normalized the average number of simulated localizations per bin by the number of cells to determine the probability to be found in a certain bin, obtaining the single random spot distance distributions and the two random spot distance distributions. We followed the same normalization for the measured data to obtain the measured distance distributions. Histograms were generated for the measured and random distance distributions. Numbers for individual bins in the distribution of the experimental data were divided by the number in the corresponding bind for the one random spot distribution to give *g(r)*. A *g(r)* value of 1 indicates no enrichment relative to a random distribution. We also divided the double random spot distribution by the single random spot distribution as a control.

Single molecule intensity and copy number analysis

Imaging was performed at room temperature on an inverted Nikon Ti2 microscope using a 100x oil objective lens (CFI APO 100x oil TIRF NA 1.49). Images were captured using an Andor iXon EM+ DU-897 EMCCD camera. Excitation was done from an OBIS 514nm LX 50mW laser delivered from an OBIS Galaxy laser beam combiner (Coherent) and a zet405/514/561x custom triple excitation set (Chroma). Laser triggering was done through a real-time controller NI DAQ (National Instruments). Experiments were done using HiLo illumination setup (Tokunaga et al., 2008) from a custom made TIRF setup. Molecular Devices MetaMorph imaging software was used to control the microscope and lasers. Videos for each strain included 500 frames. Image capture was done using continuous acquisition at 10 milliseconds frame rate (100% 515nm laser).

Initial spot positions were manually selected using the coordinates for localized bleaching in the image recorded by the acquisition software. Tracking was then done automatically using a previously developed custom program in MATLAB (Mathworks), ADEMS code (Miller et al., 2015) (freely available at https://sourceforge.net/projects/york-biophysics/). This program generated individual intensity traces. The change point detection algorithm, *ischange*, a built-in function in MATLAB was then used to find abrupt changes in the spot intensity and to determine the intensity change in the last step during bleaching (representing a single molecule). The maximum numbers of steps was restricted to 10. The intensity of the last step was used as the single molecule intensity.

An average frame projection of the videos was used to manually create single cell outlines. Individual cell were identified along with the cell lengths in pixels, the area in pixels and the total cell intensities for only the first frame of each video. To remove the endogenous cell background from our copy number calculations, the average pixel intensity was determined in AB1157 untagged cells. The single pixel background intensity was multiplied by the area of each individual cell and this total background intensity was removed from the total cell intensities. This provided the total intensity of our fluorescent protein per cell. This total intensity was divided by the single molecule intensity to give the copy number.

To determine the bound proportion, the cell background from our AB1157 measurements and the mean cell intensity for one pixel of the protein in question were removed from the first frame intensity from the single molecule intensity analysis intensity traces to get the intensity of each spot. The intensity was divided by our single molecule intensity data to get the number of molecules bound. Finally, this number was divided by the protein copy number to get the bound proportion.

SOS response assay

Strains were transformed with pEAW903, a pET21a plasmid with SuperGlo GFP (Qbiogene) under the control of the *E. coli recN* promoter (Ronayne et al., 2016). Strains were grown overnight in M63 minimal medium + 0.4% glucose supplemented with 0.2% casamino acids and ampicillin (Elbing & Brent, 2001). Overnight cultures were diluted to OD_{600} 0.05 in minimal medium or LB with ampicillin and 200uL was added to the wells (in triplicate) of a 96-well black-side clear-bottom plate (Corning). A BioTek Synergy 2 plate reader was used for taking OD_{600} and fluorescence reads (excitation 485nm /emission 528nm) during the growth curve. The plate was maintained at 37°C with shaking set to ‘slow-continuously’ and an optical adhesive cover (Applied Biosystems). Once log phase was reached, the protocol was stopped and 10μL of cells was used for serial dilution and determining CFU/mL values. The plate was immediately returned to the plate reader and a new protocol was started to capture the growth curve through stationary phase.

P1 co-transduction frequency

All transductions were performed as described (Willetts et al., 1969). Transductions were plated on 56/2 minimal medium with the selection markers noted in Table 1. Transductants were grown at 37°C (unless otherwise noted) and purified on the same type of media on which they were selected. Purified transductants were then patch plated on 56/2 or LB (corresponding to initial media used for selection) and grown at 37°C. Patch plates were then used for replica plating to screen for co-transduction of experimental mutation with the selectable marker. Screening for *recBCD* genotype was done using UV sensitivity. Replicate plates were exposed to UV using a Spectrolinker XL-1000 UV crosslinker (Spectronics Corp.) and plates were kept in the dark until analyzed. Co-transduction frequencies are scored out of total transductants confirmed to have the initial selection marker and genotype of recipient strain after replica plating.

Supplementary Material

Refer to Web version on PubMed Central for supplementary material.

Acknowledgements

We thank Dr. Jeremy Schroeder and members of the Keck, Reyes-Lamothe, and Sandler laboratories for critical evaluation of the manuscript. This work was supported by a National Institutes of Health grant to JLK and SJS (R01 GM098885) and by a National Science Foundation Graduate Research Fellowship Program to CW (DGE-1256259).

Data availability statement

The data that support the findings of this study are available from the corresponding author upon reasonable request.

References

Aguilera A, & Garcia-Muse T (2012). R loops: from transcription byproducts to threats to genome stability. Mol Cell, 46(2), 115–124. [PubMed: 22541554]

Alberts BM (1987). Prokaryotic DNA replication mechanisms. Philosophical Transactions of the Royal Society of London. Series B, Biological Sciences, Vol. 317, pp. 395–420.

Atkinson J, Gupta MK, & McGlynn P (2011). Interaction of rep and DnaB on DNA. Nucleic Acids Research, 39(4), 1351–1359. [PubMed: 20959294]

Atkinson J, Gupta MK, Rudolph CJ, Bell H, Lloyd RG, & McGlynn P (2011). Localization of an accessory helicase at the replisome is critical in sustaining efficient genome duplication. Nucleic Acids Research, 39(3), 949–957. [PubMed: 20923786]

Azvolinsky A, Giresi PG, Lieb JD, & Zakian VA (2009). Highly transcribed RNA polymerase II genes are impediments to replication fork progression in Saccharomyces cerevisiae. Molecular Cell, 34(6), 722–734. [PubMed: 19560424]

Baharoglu Z, Lestini R, Duigou S, & Michel B (2010). RNA polymerase mutations that facilitate replication progression in the rep uvrD recF mutant lacking two accessory replicative helicases. Mol Microbiol, 77(2), 324–336. [PubMed: 20497334]

Bentchikou E, Chagneau C, Long E, Matelot M, Allemand JF, & Michel B (2015). Are the SSB-interacting proteins reco, RecG, PriA and the DnaB-interacting protein rep bound to progressing replication forks in Escherichia coli PLoS ONE, 10(8).

Bhattacharyya B, George NP, Thurmes TM, Zhou R, Jani N, Wessel SR, … Keck JL (2014). Structural mechanisms of PriA-mediated DNA replication restart. Proc Natl Acad Sci U S A, 111(4), 1373–1378. [PubMed: 24379377]

Boubakri H, de Septenville AL, Viguera E, & Michel B (2010). The helicases DinG, Rep and UvrD cooperate to promote replication across transcription units in vivo. The EMBO Journal, 29(1), 145–157. [PubMed: 19851282]

Boyce RP, & Howard-Flanders P (2003). Release of ultraviolet light-induced thymine dimers from DNA in E. coli K-12. 1964. DNA Repair, 2(1927), 1280–1287. [PubMed: 15272456]

Carr KM, & Kaguni JM (1996). The A184V missense mutation of the dnaA5 and dnaA46 alleles confers a defect in ATP binding and thermolability in initiation of Escherichia coli DNA replication. Molecular Microbiology, 20, 1307–1318. [PubMed: 8809781]

Chandler M, Bird RE, & Caro L (1975). The replication time of the Escherichia coli K12 chromosome as a function of cell doubling time. Journal of Molecular Biology, 94(1), 127–132. [PubMed: 1095767]

Chen SH, Byrne RT, Wood E. a., & Cox MM (2015). Escherichia coli radD (yejH) gene: a novel function involved in radiation resistance and double-strand break repair. Molecular Microbiology, 95(January), 754–768. [PubMed: 25425430]

Cheng Z, Caillet A, Ren B, & Ding H (2012). Stimulation of Escherichia coli DNA damage inducible DNA helicase DinG by the single-stranded DNA binding protein SSB. FEBS Letters, 586(21), 3825–3830. [PubMed: 23036643]

Costes A, Lecointe F, McGovern S, Quevillon-Cheruel S, & Polard P (2010). The C-terminal domain of the bacterial SSB protein acts as a DNA maintenance hub at active chromosome replication forks. PLoS Genet, 6(12), e1001238. [PubMed: 21170359]

Crouch RJ (1990). Ribonuclease H: from discovery to 3D structure. New Biol, 2(9), 771–777. [PubMed: 2177653]

Datsenko KA, & Wanner BL (2000). One-step inactivation of chromosomal genes in Escherichia coli K-12 using PCR products. Proc Natl Acad Sci U S A, 97(12), 6640–6645. [PubMed: 10829079]

de Massy B, Fayet O, & Kogoma T (1984). Multiple origin usage for DNA replication in sdrA(rnh) mutants of Escherichia coli K-12. Initiation in the absence of oriC. Journal of Molecular Biology, 178(2), 227–236. [PubMed: 6387151]

Deshpande a M., & Newlon CS (1996). DNA replication fork pause sites dependent on transcription. Science (New York, N.Y.), 272(5264), 1030–1033.

Dimude JU, Stockum A, Midgley-Smith SL, Upton AL, Foster HA, Khan A, … Rudolph CJ (2015). The Consequences of Replicating in the Wrong Orientation: Bacterial Chromosome Duplication without an Active Replication Origin. MBio, 6(6).

Drolet M, Phoenix P, Menzel R, Masse E, Liu LF, & Crouch RJ (1995). Overexpression of RNase H partially complements the growth defect of an Escherichia coli delta topA mutant: R-loop formation is a major problem in the absence of DNA topoisomerase I. Proc Natl Acad Sci U S A, 92(8), 3526–3530. [PubMed: 7536935]

Dutta D, Shatalin K, Epshtein V, Gottesman ME, & Nudler E (2011). Linking RNA polymerase backtracking to genome instability in E. coli. Cell, 146(4), 533–543. [PubMed: 21854980]

El Hage A, French SL, Beyer AL, & Tollervey D (2010). Loss of Topoisomerase I leads to R-loop-mediated transcriptional blocks during ribosomal RNA synthesis. Genes & Development, 24(14), 1546–1558. [PubMed: 20634320]

Elbing K, & Brent R (2001). Media Preparation and Bacteriological Tools. In Current Protocols in Molecular Biology.

Epshtein V, Kamarthapu V, McGary K, Svetlov V, Ueberheide B, Proshkin S, … Nudler E (2014). UvrD facilitates DNA repair by pulling RNA polymerase backwards. Nature, 505(7483), 372–377. [PubMed: 24402227]

Finch PW, Chambers P, & Emmerson PT (1985). Identification of the *Escherichia coli recN* gene product as a major SOS protein. Journal of Bacteriology, 164(2), 653–658. [PubMed: 2997124]

French S (1992). Consequences of replication fork movement through transcription units in vivo. Science, 258(5086), 1362–1365. [PubMed: 1455232]

Frey J, Chandler M, & Caro L (1981). The initiation of chromosome replication in a dnaAts46 and a dnaA+ strain at various temperatures. Mol Gen Genet, 182(2), 364–366. [PubMed: 7026978]

Gan W, Guan Z, Liu J, Gui T, Shen K, Manley JL, & Li X (2011). R-loop-mediated genomic instability is caused by impairment of replication fork progression. Genes and Development, 25(19), 2041–2056. [PubMed: 21979917]

Glover BP, & McHenry CS (1998). The chi psi subunits of DNA polymerase III holoenzyme bind to single-stranded DNA-binding protein (SSB) and facilitate replication of an SSB-coated template. J Biol Chem, 273(36), 23476–23484. [PubMed: 9722585]

Guy CP, Atkinson J, Gupta MK, Mahdi A. a., Gwynn EJ, Rudolph CJ, … McGlynn P (2009). Rep Provides a Second Motor at the Replisome to Promote Duplication of Protein-Bound DNA. Molecular Cell, 36(4), 654–666. [PubMed: 19941825]

Harinarayanan R, & Gowrishankar J (2003). Host factor titration by chromosomal R-loops as a mechanism for runaway plasmid replication in transcription termination-defective mutants of Escherichia coli. Journal of Molecular Biology, 332(1), 31–46. [PubMed: 12946345]

Hawkins M, Dimude JU, Howard JAL, Smith AJ, Dillingham MS, Savery NJ, … McGlynn P (2019). Direct removal of RNA polymerase barriers to replication by accessory replicative helicases. Nucleic Acids Research, 47(10), 5100–5113. [PubMed: 30869136]

Helmrich A, Ballarino M, Nudler E, & Tora L (2013). Transcription-replication encounters, consequences and genomic instability. Nat Struct Mol Biol, 20(4), 412–418. [PubMed: 23552296]

Helmrich A, Ballarino M, & Tora L (2011). Collisions between replication and transcription complexes cause common fragile site instability at the longest human genes. Mol Cell, 44(6), 966–977. [PubMed: 22195969]

Hinds T, & Sandler SJ (2004). Allele specific synthetic lethality between priC and dnaAts alleles at the permissive temperature of 30°C in E. coli K-12. BMC Microbiology, 4.

Hong X, Cadwell GW, & Kogoma T (1995). Escherichia coli RecG and RecA proteins in R-loop formation. Embo J, 14(10), 2385–2392. [PubMed: 7774596]

Houlard M, Artus J, Léguillier T, Vandormael-Pournin S, & Cohen-Tannoudji M (2011). DNA-RNA hybrids contribute to the replication dependent genomic instability induced by Omcg1 deficiency. Cell Cycle, 10(1), 108–117. [PubMed: 21191184]

Hraiky C, Raymond MA, & Drolet M (2000). RNase H overproduction corrects a defect at the level of transcription elongation during rRNA synthesis in the absence of DNA topoisomerase I in Escherichia coli. J Biol Chem, 275(15), 11257–11263. [PubMed: 10753935]

Huertas P, & Aguilera A (2003). Cotranscriptionally formed DNA:RNA hybrids mediate transcription elongation impairment and transcription-associated recombination. Mol Cell, 12(3), 711–721. [PubMed: 14527416]

Itaya M, & Crouch RJ (1991). Correlation of activity with phenotypes of Escherichia coli partial function mutants of rnh, the gene encoding RNase H. Molecular & General Genetics : MGG, 227(3), 433–437. [PubMed: 1650909]

Itaya Mitsuhiro, & Crouch RJ (1991). A combination of RNase H (rnh) and recBCD or sbcB mutations in Escherichia coli K 12 adversely affects growth. MGG Molecular & General Genetics, 227, 424–432. [PubMed: 1650908]

Itoh T, & Tomizawa J (1980a). Formation of an RNA primer for initiation of replication of ColE1 DNA by ribonuclease H. Proceedings of the National Academy of Sciences of the United States of America, 77(5), 2450–2454. [PubMed: 6156450]

Itoh T, & Tomizawa J (1980b). Formation of an RNA primer for initiation of replication of ColE1 DNA by ribonuclease H. Proc Natl Acad Sci U S A, 77(5), 2450–2454. [PubMed: 6156450]

Janion C (2008). Inducible SOS response system of DNA repair and mutagenesis in Escherichia coli. International Journal of Biological Sciences, 4(6), 338–344. [PubMed: 18825275]

Jin DJ, Burgess RR, Richardson JP, & Gross C. a. (1992). Termination efficiency at rho-dependent terminators depends on kinetic coupling between RNA polymerase and rho. Proceedings of the National Academy of Sciences of the United States of America, 89(4), 1453–1457. [PubMed: 1741399]

Jin Ding Jun, Cashel M, Friedman DI, Nakamura Y, Walter WA, & Gross CA (1988). Effects of Rifampicin resistant rpoB mutations on antitermination and interaction with nusA in Escherichia coli. Journal of Molecular Biology, 204(2), 247–261. [PubMed: 2464690]

Joyce CM, Fujii DM, Laks HS, Hughes CM, & Grindley ND (1985). Genetic mapping and DNA sequence analysis of mutations in the polA gene of Escherichia coli. Journal of Molecular Biology, 186(2), 283–293. [PubMed: 3910840]

Julou T, Mora T, Guillon L, Croquette V, Schalk IJ, Bensimon D, & Desprat N (2013). Cell-cell contacts confine public goods diffusion inside Pseudomonas aeruginosa clonal microcolonies. Proceedings of the National Academy of Sciences of the United States of America, 110(31), 12577–12582. [PubMed: 23858453]

Kamarthapu V, Epshtein V, Benjamin B, Proshkin S, Mironov A, Cashel M, & Nudler E (2016). ppGpp couples transcription to DNA repair in E. Coli. Science, 352(6288), 993–996. [PubMed: 27199428]

Kitani T, Yoda K, Ogawa T, & Okazaki T (1985). Evidence that discontinuous DNA replication in Escherichia coli is primed by approximately 10 to 12 residues of RNA starting with a purine. Journal of Molecular Biology, 184(1), 45–52. [PubMed: 2411935]

Kogoma T (1994). Escherichia coli RNA polymerase mutants that enhance or diminish the SOS response constitutively expressed in the absence of RNase HI activity. Journal of Bacteriology, Vol. 176, pp. 1521–1523. [PubMed: 8113195]

Kogoma T (1997a). Stable DNA replication: interplay between DNA replication, homologous recombination, and transcription. Microbiology and Molecular Biology Reviews : MMBR, 61(2), 212–238. [PubMed: 9184011]

Kogoma T (1997b). Stable DNA replication: interplay between DNA replication, homologous recombination, and transcription. Microbiol Mol Biol Rev, 61(2), 212–238. [PubMed: 9184011]

Kogoma T, Barnard KG, & Hong X (1994). RecA, Tus protein and constitutive stable DNA replication in Escherichia coli rnhA mutants. Molecular & General Genetics : MGG, Vol. 244, pp. 557–562. [PubMed: 8078483]

Kogoma Tokio. (1978). A Novel Escherichia coli Mutant Capable of DNA Replication in the Absence of Protein Synthesis. Journal of Molecular Biology, 121(1), 55–69. [PubMed: 351189]

Kogoma Tokio, Hong X, Cadwell GW, Barnard KG, & Asai T (1993). Requirement of homologous recombination functions for viability of the Escherichia coli cell that lacks RNase HI and exonuclease V activities. Biochimie, 75, 89–99. [PubMed: 8389213]

Kogoma Tokio, & von Meyenburg K (1983). The origin of replication, oriC, and the dnaA protein are dispensable in stable DNA replication (sdrA) mutants of Escherichia coli K-12. The EMBO Journal, 2(3), 463–468. [PubMed: 11894964]

Kornberg A, & Baker TA (1992). DNA Replication (2nd ed.). New York: W. H. Freeman.

Kuzminov A (2001). Single-strand interruptions in replicating chromosomes cause double-strand breaks. Proceedings of the National Academy of Sciences of the United States of America.

Lecointe F, Serena C, Velten M, Costes A, McGovern S, Meile JC, Polard P (2007). Anticipating chromosomal replication fork arrest: SSB targets repair DNA helicases to active forks. Embo J, 26(19), 4239–4251. [PubMed: 17853894]

Li X, & Manley JL (2005). Inactivation of the SR protein splicing factor ASF/SF2 results in genomic instability. Cell, 122(3), 365–378. [PubMed: 16096057]

Lindahl G, & Lindahl T (1984). Initiation of DNA replication in Escherichia coli: RNase H-deficient mutants do not require the dnaA function. Molecular & General Genetics : MGG, 196(2), 283–289. [PubMed: 6208456]

Liu X, Wang X, Reyes-Lamothe R, & Sherratt D (2010). Replication-directed sister chromosome alignment in Escherichia coli. Mol Microbiol, 75(5), 1090–1097. [PubMed: 20487299]

Long JE, Massoni SC, & Sandler SJ (2010). RecA4142 causes SOS constitutive expression by loading onto reversed replication forks in Escherichia coli K-12. Journal of Bacteriology, 192(10), 2575–2582. [PubMed: 20304994]

Marceau AH (2012). Functions of single-strand DNA-binding proteins in DNA replication, recombination, and repair. Methods in Molecular Biology, 922, 1–21. [PubMed: 22976174]

Marceau AH, Soon B, Massoni SC, George NP, Sandler SJ, Marians KJ, & Keck JL (2011). Structure of the SSB-DNA polymerase III interface and its role in DNA replication. EMBO Journal, 30, 4236–4247.

McGlynn P, Savery NJ, & Dillingham MS (2012). The conflict between DNA replication and transcription. Mol Microbiol, 85(1), 12–20. [PubMed: 22607628]

Merrikh H, Zhang Y, Grossman AD, & Wang JD (2012). Replication-transcription conflicts in bacteria. Nature Reviews. Microbiology, 10(7), 449–458. [PubMed: 22669220]

Meyer RR, & Laine PS (1990). The single-stranded DNA-binding protein of Escherichia coli. Microbiol Rev, 54(4), 342–380. [PubMed: 2087220]

Michel B (2005). After 30 years of study, the bacterial SOS response still surprises us. PLoS Biology, 3(7), 1174–1176.

Miller H, Zhou Z, Wollman AJ, & Leake MC (2015) Superresolution imaging of single DNA molecules using stochastic photoblinking of minor groove and intercalating dyes. Methods 88:81–88. [PubMed: 25637032]

Mirkin EV, & Mirkin SM (2007). Replication fork stalling at natural impediments. Microbiology and Molecular Biology Reviews : MMBR, 71(1), 13–35. [PubMed: 17347517]

Monk M, & Kinross J (1972). Conditional lethality of recA and recB derivatives of a strain of Escherichia coli K-12 with a temperature-sensitive deoxyribonucleic acid polymerase I. J. Bacteriol, 109234, 971–978.

Moolman MC, Krishnan S. T. iruvad., Kerssemakers JWJ, van den Berg A, Tulinski P, Depken M, … Dekker NH (2014). Slow unloading leads to DNA-bound β2-sliding clamp accumulation in live Escherichia coli cells. Nature Communications, 5, 5820.

Nguyen HD, Yadav T, Giri S, Saez B, Graubert TA, & Zou L (2017). Functions of Replication Protein A as a Sensor of R Loops and a Regulator of RNaseH1. Molecular Cell, 65(5), 832–847.e4. [PubMed: 28257700]

O'Donnell M, Langston L, & Stillman B (2013). Principles and concepts of DNA replication in bacteria, archaea, and eukarya. Cold Spring Harbor Perspectives in Biology, 5(7).

Ogawa T, & Okazaki T (1980). Discontinuous DNA replication. Annu Rev Biochem, 49, 421–457. [PubMed: 6250445]

Ogawa T, & Okazaki T (1984). Function of RNase H in DNA replication revealed by RNase H defective mutants of Escherichia coli. Molecular & General Genetics : MGG, 193(2), 231–237. [PubMed: 6319961]

Ogawa T, Pickett GG, Kogoma T, & Kornberg A (1984). RNase H confers specificity in the dnaA-dependent initiation of replication at the unique origin of the Escherichia coli chromosome in vivo and in vitro. Proceedings of the National Academy of Sciences of the United States of America, 81(4), 1040–1044. [PubMed: 6322184]

Parajuli S, Teasley DC, Murali B, Jackson J, Vindigni A, & Stewart SA (2017). Human ribonuclease H1 resolves R-loops and thereby enables progression of the DNA replication fork. Journal of Biological Chemistry, 292(37), 15216–15224.

Petzold C, Marceau AH, Miller KH, Marqusee S, & Keck JL (2015). Interaction with single-stranded DNA binding protein stimulates Escherichia coli ribonuclease HI enzymatic activity. Journal of Biological Chemistry, jbc.M115.655134.

Pomerantz RT, & O'Donnell M (2010). What happens when replication and transcription complexes collide? Cell Cycle (Georgetown, Tex.), 9(13), 2537–2543.

Prado F, & Aguilera A (2005). Impairment of replication fork progression mediates RNA polII transcription-associated recombination. Embo J, 24(6), 1267–1276. [PubMed: 15775982]

Proshkin S, Rahmouni AR, Mironov A, & Nudler E (2010). Cooperation between translating ribosomes and RNA polymerase in transcription elongation. Science, 328(5977), 504–508. [PubMed: 20413502]

Reyes-Lamothe R (2012). Use of fluorescently tagged SSB proteins in in vivo localization experiments. Methods in Molecular Biology, 922, 245–253. [PubMed: 22976192]

Reyes-Lamothe R, Nicolas E, & Sherratt DJ (2012). Chromosome replication and segregation in bacteria. Annual Review of Genetics, 46, 121–143.

Reyes-Lamothe R, Possoz C, Danilova O, & Sherratt DJ (2008). Independent positioning and action of Escherichia coli replisomes in live cells. Cell, 133(1), 90–102. [PubMed: 18394992]

Reyes-Lamothe R, Sherratt DJ, & Leake MC (2010). Stoichiometry and architecture of active DNA replication machinery in Escherichia coli. Science, 328(5977), 498–501. [PubMed: 20413500]

Ronayne EA, Wan YCS, Boudreau BA, Landick R, & Cox MM (2016). P1 Ref Endonuclease: A Molecular Mechanism for Phage-Enhanced Antibiotic Lethality. PLoS Genetics, 12(1).

Rostas K, Morton SJ, Picksley SM, & Lloyd RG (1987). Nucleotide sequence and LexA regulation of the Escherichia coli recN gene. Nucleic Acids Research, 15(13), 5041–5049. [PubMed: 3037486]

Sanders K, Lin CL, Smith AJ, Cronin N, Fisher G, Eftychidis V, … Dillingham MS (2017). The structure and function of an RNA polymerase interaction domain in the PcrA/UvrD helicase. Nucleic Acids Research, 45(7), 3875–3887. [PubMed: 28160601]

Sandler SJ (2005). Requirements for replication restart proteins during constitutive stable DNA replication in Escherichia coli K-12. Genetics, 169(4), 1799–1806. [PubMed: 15716497]

Sandler SJ, Samra HS, & Clark AJ (1996). Differential suppression of priA2::kan phenotypes in Escherichia coli K-12 by mutations in priA, lexA, and dnaC. Genetics, 143(1), 5–13. [PubMed: 8722757]

Sandler Steven J., McCool JD, Do TT, & Johansen RU (2001). PriA mutations that affect PriA-PriC function during replication restart. Molecular Microbiology, 41(3), 697–704. [PubMed: 11532137]

Shaner NC, et al. (2013) A bright monomeric green fluorescent protein derived from Branchiostoma lanceolatum. Nat Methods 10(5):407–409. [PubMed: 23524392]

Shereda RD, Kozlov AG, Lohman TM, Cox MM, & Keck JL (2008). SSB as an organizer/mobilizer of genome maintenance complexes. Crit Rev Biochem Mol Biol, 43(5), 289–318. [PubMed: 18937104]

Sliusarenko O, Heinritz J, Emonet T, & Jacobs-Wagner C (2011). High-throughput, subpixel precision analysis of bacterial morphogenesis and intracellular spatio-temporal dynamics. Mol Microbiol, 80(3), 612–627. [PubMed: 21414037]

Soubry N, Wang A, & Reyes-Lamothe R (2019). Replisome activity slowdown after exposure to ultraviolet light in Escherichia coli. Proceedings of the National Academy of Sciences of the United States of America, 116(24), 11747–11753. [PubMed: 31127046]

Srivatsan A, Tehranchi A, MacAlpine DM, & Wang JD (2010). Co-orientation of replication and transcription preserves genome integrity. PLoS Genetics, 6(1), e1000810. [PubMed: 20090829]

Stylianidou S, Brennan C, Nissen SB, Kuwada NJ, & Wiggins PA (2016). SuperSegger: robust image segmentation, analysis and lineage tracking of bacterial cells. Molecular Microbiology, 102(4), 690–700. [PubMed: 27569113]

Sun W, & Godson GN (1996). Interaction of Escherichia coli primase with a phage G4ori(c)-E. coli SSB complex. J Bacteriol, 178(23), 6701–6705. [PubMed: 8955285]

Syeda AH, Wollman AJM, Hargreaves AL, Howard JAL, Brüning J-G, McGlynn P, & Leake MC (2019). Single-molecule live cell imaging of Rep reveals the dynamic interplay between an accessory replicative helicase and the replisome. Nucleic Acids Research, 47(12), 6287–6298. [PubMed: 31028385]

Tehranchi AK, Blankschien MD, Zhang Y, Halliday JA, Srivatsan A, Peng J, … Wang JD (2010). The transcription factor DksA prevents conflicts between DNA replication and transcription machinery. Cell, 141(4), 595–605. [PubMed: 20478253]

Thrall ES, Kath JE, Chang S, & Loparo JJ (2017). Single-molecule imaging reveals multiple pathways for the recruitment of translesion polymerases after DNA damage. Nature Communications, 8(1).

Tokunaga M, Imamoto N, & Sakata-Sogawa K (2008) Highly inclined thin illumination enables clear single-molecule imaging in cells. Nat Methods 5(2):159–161. [PubMed: 18176568]

Trautinger BW, Jaktaji RP, Rusakova E, & Lloyd RG (2005). RNA polymerase modulators and DNA repair activities resolve conflicts between DNA replication and transcription. Molecular Cell, 19(2), 247–258. [PubMed: 16039593]

Tuduri S, Crabbé L, Conti C, Tourrière H, Holtgreve-Grez H, Jauch A, Pasero P (2009). Topoisomerase I suppresses genomic instability by preventing interference between replication and transcription. Nature Cell Biology, 11(11), 1315–1324. [PubMed: 19838172]

Uphoff S, Reyes-Lamothe R, De Leon FG, Sherratt DJ, & Kapanidis AN (2013). Single-molecule DNA repair in live bacteria. Proceedings of the National Academy of Sciences of the United States of America, 110(20), 8063–8068. [PubMed: 23630273]

Uyemura D, & Lehman I (1976). Biochemical characterization of mutant forms of DNA polymerase I from Escherichia coli. I. The polA12 mutation. The Journal of Biological Chemistry, 251(13), 4078–4084. [PubMed: 6470]

Vilette D, Ehrlich DS, & Michel B (1996). Transcription-induced deletions in plasmid vectors: M13 DNA replication as a source of instability. Molecular and General Genetics, 252(4), 398–403. [PubMed: 8879240]

von Meyenburg K, Boye E, Skarstad K, Koppes L, & Kogoma T (1987). Mode of initiation of constitutive stable DNA replication in RNase H-defective mutants of Escherichia coli K-12. J Bacteriol, 169(6), 2650–2658. [PubMed: 3034862]

Wahba L, Amon JD, Koshland D, & Vuica-Ross M (2011). RNase H and multiple RNA biogenesis factors cooperate to prevent RNA:DNA hybrids from generating genome instability. Mol Cell, 44(6), 978–988. [PubMed: 22195970]

Walker GC, Smith BT, and Sutton MD (2000). The SOS response to DNA damage. In Storz R, Hengge-Aronis G (Ed.), Bacterial Stress Responses (pp. 131–144). American Society of Microbiology Press.

Wang JD, Berkmen MB, & Grossman AD (2007). Genome-wide coorientation of replication and transcription reduces adverse effects on replication in Bacillus subtilis. Proc Natl Acad Sci U S A, 104(13), 5608–5613. [PubMed: 17372224]

Washburn RS, & Gottesman ME (2011). Transcription termination maintains chromosome integrity. Proc Natl Acad Sci U S A, 108(2), 792–797. [PubMed: 21183718]

Wessel SR, Marceau AH, Massoni SC, Zhou R, Ha T, Sandler SJ, & Keck JL (2013). PriC-mediated DNA replication restart requires PriC complex formation with the single-stranded DNA-binding protein. J Biol Chem, 288, 17569–17578. [PubMed: 23629733]

Westover KD, Bushnell D. a, & Kornberg RD (2004). Structural basis of transcription: separation of RNA from DNA by RNA polymerase II. Science (New York, N.Y.), 303(5660), 1014–1016.

Willetts NS, Clark a. J., & Low B (1969). Genetic location of certain mutations conferring recombination deficiency in Escherichia coli. Journal of Bacteriology, 97(1), 244–249. [PubMed: 4884815]

Zawadzki P, Stracy M, Ginda K, Zawadzka K, Lesterlin C, Kapanidis AN, & Sherratt DJ (2015). The Localization and Action of Topoisomerase IV in Escherichia coli Chromosome Segregation Is Coordinated by the SMC Complex, MukBEF. Cell Reports, 13(11), 2587–2596. [PubMed: 26686641]

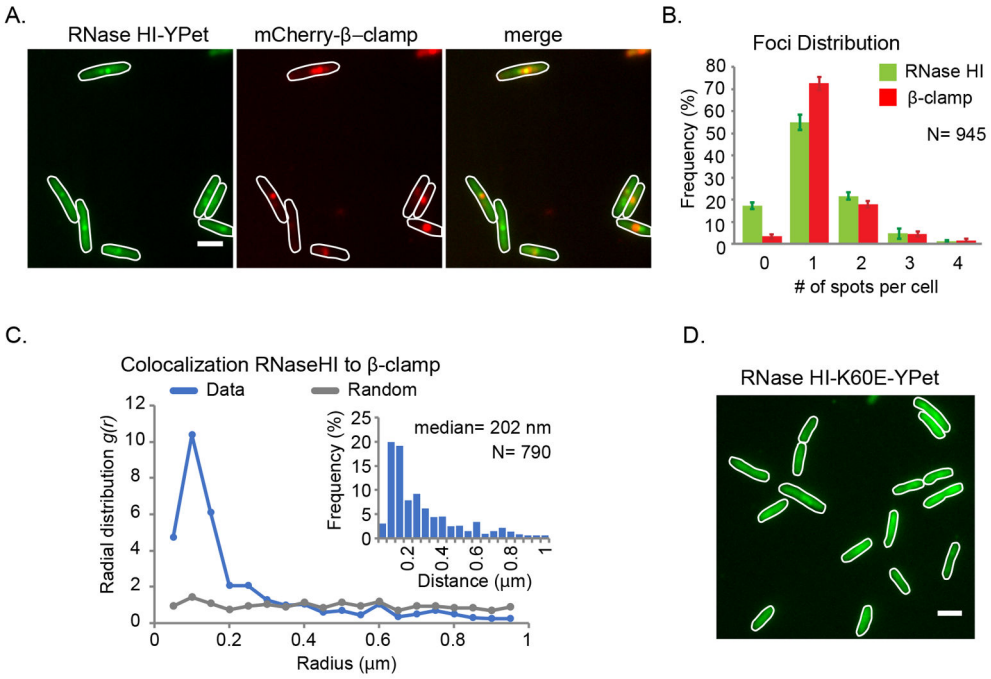

Figure 1. SSB-mediated localization of RNase HI to the replication fork.

Fluorescence microscopy studies of *E. coli* strains expressing the fluorescent fusion proteins RNase HI-YPet and β-clamp-mCherry. **(A)** Representative images showing RNase HI-YPet (left), β-clamp-mCherry (middle) and a merged image showing the overlap of RNase HI-YPet and β-clamp-mCherry (right) in strain VV11. Digital contrast enhancement was used for presentation purposes. Scale bar in the right image is 2 μm. **(B)** Detectable RNase HI-YPet and β-clamp-mCherry foci per cell are plotted as the frequency for the cell population. **(C)** Radial distribution function for RNase HI-YPet and β-clamp-mCherry representing colocalization (blue line). As comparison, *g(r)* is plotted for a set of randomly distributed spots in cells (grey line). Inset shows the distribution of nearest-neighbor distances between spots of RNase HI-YPet and β-clamp-mCherry. **(D)** Representative fluorescent image of showing RNase HI K60E-YPet fusion protein distributed throughout strain VV08. Imaging conditions and digital contrast enhancement used were as in 1B. Scale bar is 2 μm.

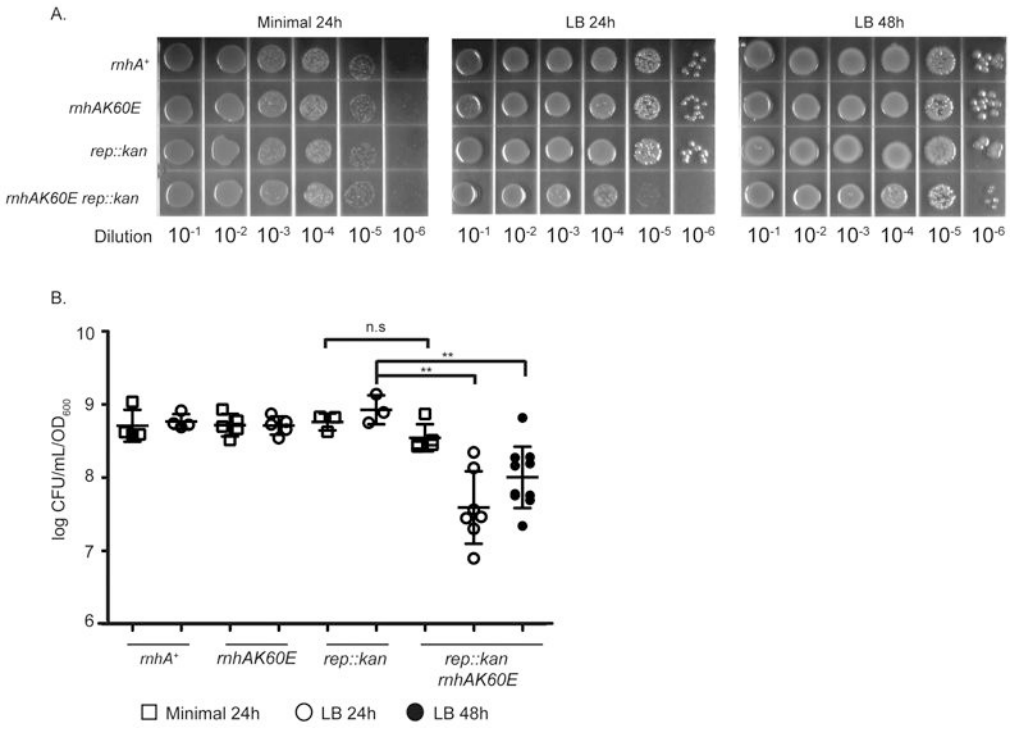

Figure 2. The *rnhAK60E rep::kan* strain is sensitive to growth on rich medium plates.

(A) Dilutions of overnight cultures grown in minimal medium (56/2) and plated on minimal (left) or LB media (middle and right). Plates were incubated at 37°C for 24 or 48 hours. The images are representative of plating experiments performed in triplicate. Strains are CP65, CP58, CP84, and CP86 from top to bottom. **(B & C)** The CFU/mL of each strain (normalized to OD_{600}) is plotted from overnight cultures diluted and plated on minimal (squares) or LB (circles) media. Colonies were quantitated after growth at 37°C for 24 or 48 hours. Each symbol is a single culture and the mean CFU/mL for each strain is represented by a black line. Strains are CP65, CP58, CP84, and CP86 from left to right. Error bars indicate the standard deviation. ** = p-value < 0.005 and n.s = p-value > 0.05 using two-tailed t-test.

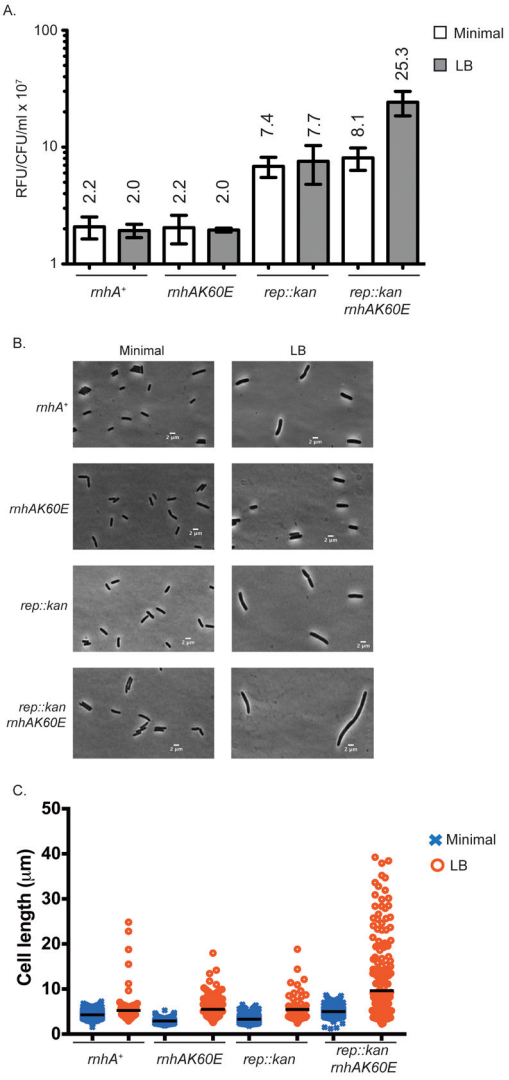

Figure 3. The *rnhAK60E rep::kan* strain has elevated SOS levels in rich medium.

(A) The relative fluorescent units (RFU) from plasmid-borne GFP driven by a *recN* promoter is plotted for each strain at mid-log phase and normalized to CFU/mL at the time of data collection. Bars represent the mean RFU/CFU/mL from biological and technical replicates of strains were grown in minimal medium (56/2) and LB. Error bars display the standard deviation of the mean. Mean values are written above each bar. Strains in this figure are CP127, CP128, CP129, and CP126 (from left to right). **(B)** Representative phase contrast images from strains grown in minimal medium (left) or LB (right). The strains were grown to early log phase and subsequently spotted on 2% agarose pads for imaging using a Nikon Eclipse Ti microscope equipped with a Photometrics CoolSNAP HQ2 charge-coupled-device (CCD) camera. **(C)** The cell lengths captured by MATLAB of microscope images. Cells were grown in minimal medium or LB and treated as in (B).

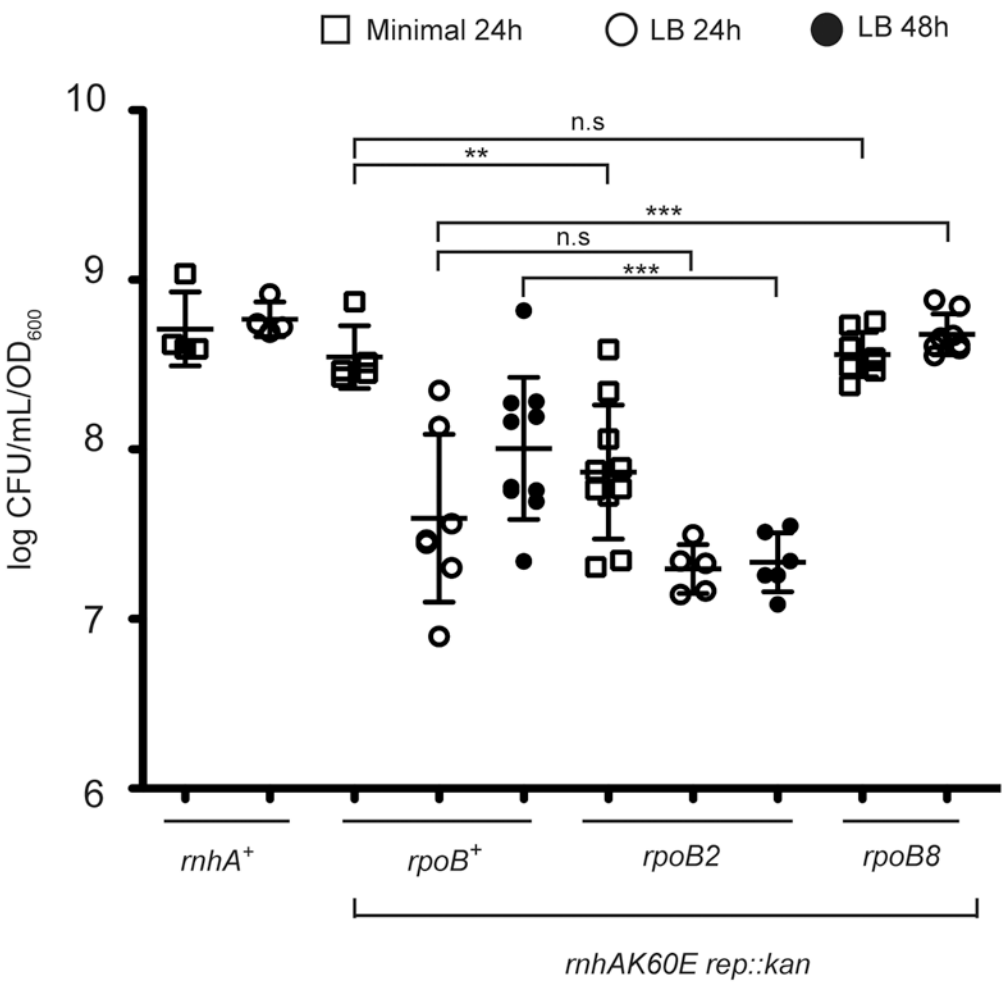

Figure 4. The plating efficiency of *rnhAK60E rep::kan rpoB* mutants on minimal and rich media.

The CFU/mL of each strain (normalized to OD_{600}) is plotted from overnight cultures diluted and plated on minimal (squares) or LB (circles) media. Colonies were quantitated after growth at 37°C for 24 or 48 hours. Each symbol is a single culture and the mean CFU/mL for each strain is represented by a black line. The strains are CP65, CP86, CP119, and CP124 from left to right. The error bars indicate the standard deviation. Significant difference levels (p-values) were determined between *rnhAK60E rep::kan* strains +/− *rpoB* mutants grown in the same medium using two-tailed t-test. * = p-value < 0.05; ** = p-value < 0.005; *** = p-value < 0.0005; n.s = p-value > 0.05

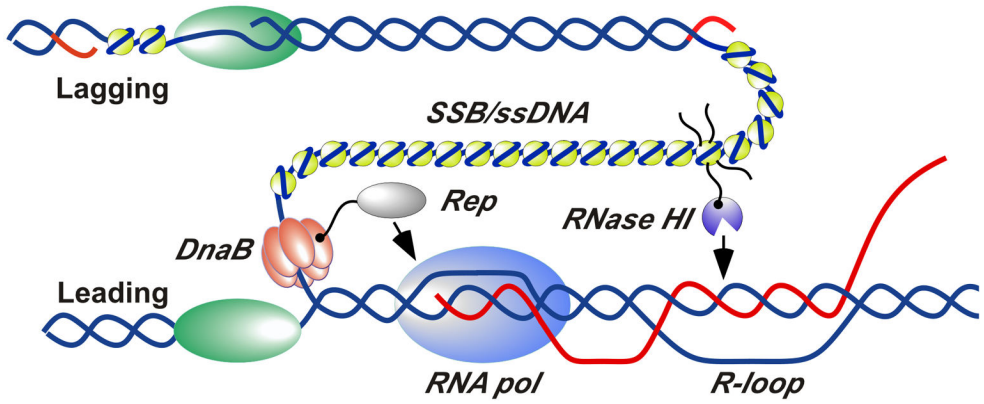

Figure 5. Schematic model for RNase HI and Rep helicase localization and action at sites of replication/transcription collision.

RNase HI (purple) is localized to the DNA replication fork by interaction with SSB (yellow). Rep helicase (grey) is localized by interaction with DnaB (orange). SSB-Ct tails are shown explicitly for only one SSB tetramer for clarity. DNA strands are shown in blue, RNA strands are shown in red, and DNA polymerases are shown in green. Several replisome components have been omitted or separated for clarity.

Table 1.

Co-transduction analysis to determine the synthetic lethality of helicase mutations with *rnhAK60E*

	Donor Strain (relevant genotype)	**Recipient Strain (relevant genotype)**	**Results (Screen/Selection)**
(a) Rep	SS9364 (*rep::kan ilv*$^+$)	CP70 (*rnhA*$^+$*, cat ilv-500::Tn10*)	86/101 (Kan^r /ilv$^+$)
	SS9364 (*rep::kan ilv*$^+$*)*	CP60 (*rnhAK60E, cat ilv-500::Tn10*)	54/77 (Kan^r /ilv$^+$)
	SS9364 (*rep::kan ilv*$^+$)	SS9180 (*rnhA::cat ilv-500::Tn10)*	0/57 (Kan^r /ilv$^+$)
	CP165 (*rnhA::cat zae502::Tn10*)	CP65 (*rnhA*$^+$*)*	17/56 (Cm^r/Tc^r)
	CP165 (*rnhA::cat zae502::Tn10*)	CP84 (*rep::kan)*	21/54 (Cm^r/Tc^r)
(b) RecBCD	SS6046 (*recBCD::cat proA*$^+$)	JC13509 (*rnhA*$^+$ proA−)	30/30 (Cm^r/proA$^+$)
	SS6046 (*recBCD::cat proA*$^+$)	CP62 (*rnhAK60E proA::kan)*	28/30 (Cm^r/proA$^+$)
	SS6046 (*recBCD::cat proA*$^+$)	SS10032 (*rnhA::cat del(proA)kan)*	0/41 (UV^S /proA$^+$) *
	SS10032 (*rnhA::cat del(proA)kan*)	JC13509 (*rnhA*$^+$*)*	6/46 (Cm^r/Kan^r)
	SS10032 (*rnhA::cat del(proA)kan*)	SS7329 *(recB270(ts) recC271(ts)*)	0/42 (Cm^r /Kan^r) **
(c) RecG	CP79 (*recG(kan ins) zic-4901::Tn10*)	CP63 (*rnhA*$^+$*, cat*)	52/54 (Kan^r/Tc^r)
	CP79 (*recG(kan ins) zic-4901::Tn10*)	CP54 (*rnhAK60E, cat)*	44/54(Kan^r/Tc^r)
	CP79 (*recG(kan ins) zic-4901::Tn10*)	CP154 (*rnhA::cat*)	0/53 (Kan^r/Tc^r)
	CP165 (*rnhA::cat zae502::Tn10*)	CP64 (*recG(kan ins))*	0/12 (Cm^r/Tet^r)
(d) UvrD	CP95 (*uvrD::kan fadAB101::Tn10*)	CP63 (*rnhA*$^+$*, cat*)	23/103 (Kan^r/Tc^r)
	CP95 (*uvrD::kan fadAB101::Tn10*)	CP54 (*rnhAK60E, cat)*	27/103 (Kan^r/Tc^r)
	CP95 (*uvrD::kan fadAB101::Tn10*)	SS1651 (*rnhA339::cat)*	0/104 (Kan^r/Tc^r)
	CP165 (*rnhA::cat zae502::Tn10*)	CP88 (*uvrD::kan)*	0/58 (Cm^r/Tc^r)
(e) DinG	CP96 (*dinG::kan zbi-29::Tn10*)	CP63 (*rnhA*$^+$*, cat*)	23/31 (Kan^r/Tc^r)
	CP96 (*dinG::kan zbi-29::Tn10*)	CP54 (*rnhAK60E, cat)*	27/44 (Kan^r/Tc^r)
	CP96 (*dinG::kan zbi-29::Tn10*)	CP154 (*rnhA::cat*)	30/48 (Kan^r/Tc^r)

* PCR to confirm *rnhA* locus and test *recBCD* genotype with UV sensitivity

** Selection at 30°C, screen at 42°C